Dalton Transactions

Accepted Manuscript

This is an *Accepted Manuscript*, which has been through the Royal Society of Chemistry peer review process and has been accepted for publication.

Accepted Manuscripts are published online shortly after acceptance, before technical editing, formatting and proof reading. Using this free service, authors can make their results available to the community, in citable form, before we publish the edited article. We will replace this *Accepted Manuscript* with the edited and formatted *Advance Article* as soon as it is available.

You can find more information about *Accepted Manuscripts* in the Information for Authors.

Please note that technical editing may introduce minor changes to the text and/or graphics, which may alter content. The journal's standard Terms & Conditions and the Ethical guidelines still apply. In no event shall the Royal Society of Chemistry be held responsible for any errors or omissions in this *Accepted Manuscript* or any consequences arising from the use of any information it contains.

ROYAL SOCIETY OF CHEMISTRY

www.rsc.org/dalton

Growth characteristics of Ti-based fumaric acid hybrid thin films by molecular layer deposition

Yan-Qiang Cao, Lin Zhu, Xin Li, Zheng-Yi Cao, Di Wu, and Ai-Dong Li*

National Laboratory of Solid State Microstructures and Department of Materials Science and Engineering, College of Engineering and Applied sciences, Collaborative Innovation Center of Advanced Microstructures, Nanjing University, Nanjing 210093, People's Republic of China. adli@nju.edu.cn

ABSTRACT

Ti-based fumaric acid hybrid thin films were successfully prepared using inorganic $TiCl_4$ and organic fumaric acid as precursors by molecular layer deposition (MLD). The effect of deposition temperatures from 180 °C to 350 °C on the growth rate, composition, chemical state, and topology of hybrid films has been investigated systematically by means of a series of analytical tools such as spectroscopic ellipsometry, atomic force microscopy (AFM), high resolution X-ray photoelectron spectroscopy (XPS) and Fourier transform infrared spectroscopy (FTIR). The MLD process of the Ti-fumaric acid shows self-limiting surface reaction with a reasonable growth rate of ~0.93 Å per cycle and small surface roughness of ~0.59 nm in root-mean-square value at 200 °C. A temperature-dependent growth characteristic has been observed in hybrid films. With raising temperature from 180 °C to 300 °C, the growth rate decreases from 1.10 to 0.49 Å/cycle and the film XPS composition of C:O:Ti ratio changes from 8.35:7.49:1.00 to 4.66:4.80:1.00. FTIR spectra indicate the hybrid films show bridging bonding mode at low deposition temperature of 200 °C and bridging/bidentate mixture bonding mode at elevated deposition temperature of 250 and 300 °C. The higher C and O amount deviated

Dalton Transactions Accepted Manuscript

from ideal composition may be ascribed to the more organic incorporation into the hybrid films at lower deposition and temperature-dependent density of reactive sites (-OH). The composition of hybrid films grown at 350 °C show a dramatic decrease in C and O elements (C: O: Ti=1.97:2.76:1.00) due to the thermal decomposition of fumaric acid precursor. The produced by-product H_2O changes the structure of hybrid films, resulting in the formation of more Ti-O bonds at high temperature. The stability of hybrid films against chemical and thermal treatment, and long-time storage by vacuum-packing was explored carefully. It is found that the ultrathin hybrid film can be transformed into TiO_2 nanoparticles via various post deposition annealing with different topographies. Finally, the charge trapping ability of the hybrid film is confirmed by a charge trapping memory capacitor in which the hybrid film was inserted as a charge trapping layer.

KEYWORDS: molecular layer deposition, organic-inorganic hybrid films, fumaric acid, TiO_2 nanoparticles, charge trapping memory

1. INTRODUCTION

Atomic layer deposition (ALD) is a special chemical vapor deposition (CVD) technique suitable for manufacturing inorganic material layers with thickness down to the precision of a monolayer.[1,2] This technique is currently used for a wide range of materials and purposes.[3,4] Recently, the relatively new class of organic-inorganic hybrid materials has been deposited by ALD with excellent results.[5-25] In addition, this technique is frequently called as molecular layer deposition (MLD) rather than ALD due to the molecular nature of the deposition process. Regardless of the terminology, the basic mechanism of this technique is growth through self-limiting reaction between precursors in the gas phase and active sites on the solid surface.

Dalton Transactions Accepted Manuscript

Organic-inorganic hybrid materials usually possess distinct properties from both inorganic and organic components. The organic component offers ease of processing, structural flexibility, photoconductivity, etc., whereas the inorganic component provides potential for high carrier mobility, thermal and mechanical stability, etc. Hence hybrid thin films benefit from the chemistry of both constituents and may exhibit interesting properties as a whole.[11,16,26-27] Because of these advantages, organic-inorganic hybrid films have been adopted in various applications, such as optical devices,[28] photoluminescence,[29-31] protective coatings,[32] catalysis,[28] sensors,[28] optoelectronic devices,[33-39] field-effect transistors,[34,40-42] electroluminescence,[43] light emitting diodes,[41] etc.

Plenty of organic-inorganic hybrid films have been synthesized successfully by MLD. These hybrid films can be described as "metalcones", such as alucones,[7,8,11,13-15,18,22,23] zincones,[9,10] titanicones,[17,19,20,21,24] zircons,[25] etc. Among them, the titanicones films have the potential for a wide variety of applications. These titanicones films could be useful to fabricate flexible multilayer gas diffusion barriers for organic electronics and thin film solar applications.[44] Because of its similarity with TiO_2, titanicones films may also have catalytic and photocatalytic properties.[45] Porous TiO_2 frameworks formed by the annealing of titanicones films may serve as catalytic supports. The resulting porous TiO_2 films could serve as TiO_2 scaffolds for dye-sensitized solar cells or photocatalytic membranes.[20, 46]

In this work, a new kind of Ti-based organic-inorganic hybrid films was prepared using $TiCl_4$ and fumaric acid as precursors by MLD. The effect of deposition temperatures on the growth rate, morphology, composition, and chemical state of hybrid films has been

Dalton Transactions Accepted Manuscript

investigated by means of a series of analytical tools systematically. The possible growth mechanism for titanicones films has been proposed. The stability of hybrid film against chemical and thermal treatment, and long-time sealed-storage was also explored. The charge trapping ability of the hybrid films was examined in charge trapping memories.

2. EXPERIMENTAL SECTION

The Ti-fumaric acid hybrid thin films were deposited in a commercial flow-type hot-wall ALD reactor (Picosun SUNALE^{TM} R-200B) using $TiCl_4$ (99%, Nanjing Chemical Reagent CO. LTD) and trans-butene dioic acid (fumaric acid, COOH-CH=CH-COOH, 99%, Alfa Aesar) as precursors. The inorganic precursor $TiCl_4$ and the organic precursor fumaric acid were evaporated at room temperature and 172 °C, respectively. Pure N_2 (99.999%) was used as carrier gas and purging gas. The Ti-fumaric acid hybrid thin films were deposited on p-Si(100) using the pulse sequence of 0.3 s $TiCl_4$/4 s N_2 purging/2 s fumaric acid/10 s N_2 purging. Relatively long purges were adopted to make sure that there was only one precursor at a time in the ALD reactor chamber. The deposition temperature was varied from 180 °C to 350 °C with 200 deposition cycles.

Chemical and thermal treatments were carried out to explore the stability of hybrid films. The chemical treatment was performed by immerging the hybrid films into pure acetone, ethanol, isopropanol and deionized water for 1 h, respectively. In order to explore the thermal stability of the hybrid films, they were annealed at 400, 600 and 850 ^{o}C in air using rapid thermal annealing (RTA) under atmospheric pressure, and the duration time and ramp rate is 10 s and 50 °C/s, respectively. Post-deposition annealing (PDA) was performed at 850 ^{o}C in air ambient to transform the hybrid films into

Dalton Transactions Accepted Manuscript

nanoparticles by conventional tube furnace annealing (CFA) or RTA. The duration time and ramp rate is 30 min and 30 °C/min for CFA, and 10 s and 50 °C/s for RTA, respectively.

Thermogravimetric and differential scanning calorimeter (TG/DSC) analyses were performed to determine the evaporation characteristics of the molecular precursor of fumaric acid (TG/DSC, Netzsch STA 409PC/PG) under atmospheric pressure. Approximately 8 mg of fumaric acid was loaded into an alumina crucible pan and heated from room temperature to 300 °C with a ramp rate of 10 ^{o}C/min in N_2 (99.999%). The gas chromatography-mass spectrometry (GC-MS, 7890A-5975C, Agilent) was used to characterize the thermal-stability of fumaric acid at high temperature. The film thickness was measured by the *ex-situ* spectroscopic ellipsometry measurement (GES-5, Sopra). The topography and surface roughness of the hybrid films was recorded by atomic force microscopy (AFM, Cypher, Asylum Research). The root-mean-square (RMS) roughness values were obtained in 3 μm×3 μm by AFM. The crystallinity were characterized by means of X-ray diffraction (XRD, D/max 2000, Rigaku) using Cu Kα radiation (λ = 1.5406 Å) and a transmission electron microscope (TEM, Tecnai G^2 F20 S-Twin, FEI) operating at 200 kV. The chemical behavior of the films were investigated by *ex situ* X-ray photoelectron spectroscopy (XPS, Thermo Fisher K-Alpha) with standard Al Kα (1486.7eV) X-ray source. XPS was performed at a take-off angle of 90°, and the binding energy scale was calibrated using the energy position of the adventitious C 1*s* peak at 284.6 eV. In addition, the atomic ratio from XPS data were calculated based on the area underneath the peaks after subtracting the background correctly and taking the relative sensitivity factor into account. Hybrid films deposited on double sided polished Si were

Dalton Transactions Accepted Manuscript

analyzed with Fourier transform infrared spectroscopy (FTIR, Spectrum, PerkinElmer). Pristine Si substrate was used as reference. Pt top electrodes of area 1.55×10^{-4} cm^2 were deposited using a shadow mask by sputtering method for electrical measurements. The electrical characteristics of charge trapping capacitor were measured at a high frequency (1 MHz) by means of semiconductor characterization system (Keithley 4200-SCS) with a probe platform (Cascade summit 12000B-M).

3. RESULTS AND DISCUSSION

3.1. Growth and Morphology of Ti-fumaric Acid Hybrid Films by MLD.

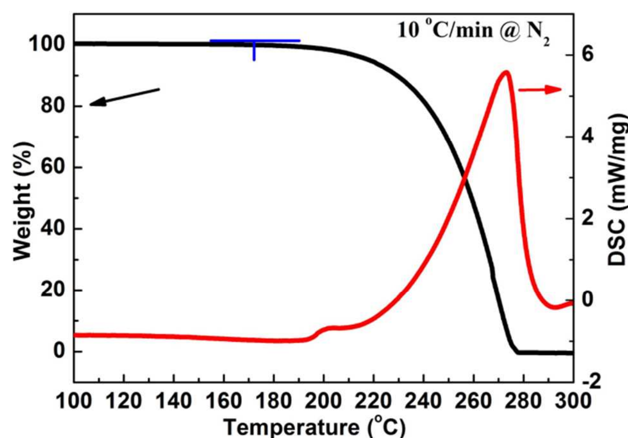

Figure 1. TG/DSC curves of the fumaric acid from room temperature to 300 °C at a heating rate of 10 °C/min in flowing N_2.

Figure 1 shows the TG/DSC curves of fumaric acid from room temperature to 300 °C at a heating rate of 10 °C/min in flowing N_2. It can be seen that fumaric acid begins to volatilize slowly at about 172 °C and the volatilization rate becomes quick at above 200 °C. A strong endothermic peak at 273 °C is attributed to the sublimation of fumaric acid in atmospheric pressure N_2. Fumaric acid source evaporates completely when the temperature reaches 277 °C. It can be found that there is no obvious thermal

Dalton Transactions Accepted Manuscript

decomposition of fumaric acid below 277 °C. The volatilization rate of fumaric acid at constant temperature of 172 °C in N_2 is examined to be 1.28×10^{-2} mg/min (Figure S1, Supporting Information). In the following ALD experiment, the source temperature of fumaric acid was set at 172 °C.

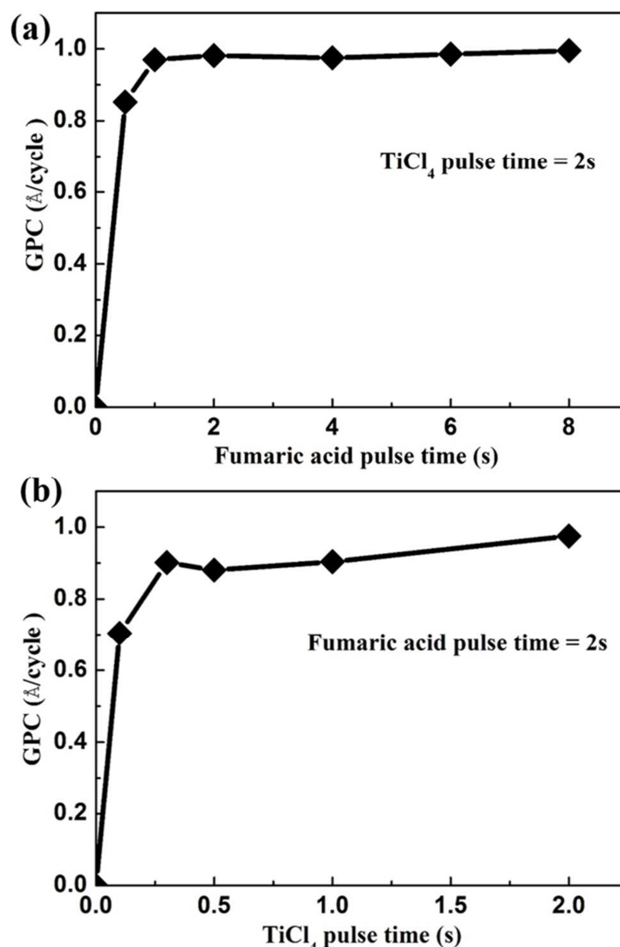

Figure 2. GPC values for Ti-fumaric acid hybrid films deposited at 200 °C as a function of (a) fumaric acid and (b) $TiCl_4$ pulse time.

The growth per cycle (GPC) is an important value to characterize the ALD reaction and growth mechanism, which was determined by measuring the film thickness after some growth cycles. The effect of the precursor pulse time of $TiCl_4$ and fumaric acid on

Dalton Transactions Accepted Manuscript

the GPC values for Ti-fumaric acid hybrid films deposited at 200 ^{o}C for 200 cycles has been examined, as illustrated in Figure 2. In Figure 2(a), the pulse length of fumaric acid source changed from 0.5 s to 8 s. While the $TiCl_4$ pulse time was set at 2 s so as to make sure that a surplus of $TiCl_4$ was introduced during the $TiCl_4$ pulse. It can be observed that the GPC value first increases with the pulse time of fumaric acid extending to 2 s and then remains constant after pulse time longer than 2 s. Similarly, the pulse time of $TiCl_4$ source varied from 0.1 s to 2 s with a fumaric acid pulse time of 2 s. The GPC value basically keeps unchanged when the $TiCl_4$ pulse length reaches 0.3 s in Figure 2(b). The MLD process of the Ti-fumaric acid hybrid films derived from $TiCl_4$ and fumaric acid shows self-limiting surface reaction at 200 ^{o}C. After the above experiments, the optimal MLD growth sequence for the Ti-fumaric acid hybrid films was fixed to 0.3 s $TiCl_4$ pulse/4 s N_2 purging/2 s fumaric acid pulse/10 s N_2 purging.

The influence of deposition temperature on the GPC values of Ti-fumaric acid hybrid thin films for 200 cycles has also been investigated, as seen in Figure 3(a). The GPC value decreases from 1.10 to 0.52 Å/cycle when increasing the deposition temperature from 180 to 350 °C. It can be seen that the deposition rate is temperature-dependant for Ti-fumaric acid system. The relatively steady growth rate of about 0.93±0.033 Å/cycle appears in the narrow temperature range of 200-220 °C. Then GPC value declines rapidly between 220 and 300 °C. The temperature dependence of GPC is similar to earlier results on hybrid films of alucones and zincones.[7,10,15] The reduction in deposition rate at higher temperatures can be ascribed to the increased thermal motion and desorption of molecules on growth surface.[19,14,47] When the temperature rises to 350 °C, the deposition rate keeps slight increment, indicating the possible occurrence of fumaric acid

Dalton Transactions Accepted Manuscript

decomposition.

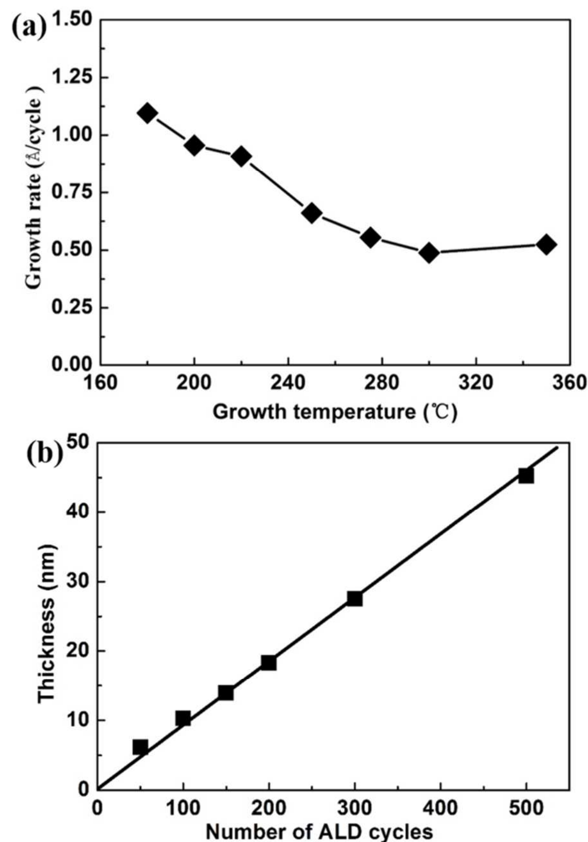

Figure 3. (a) GPC values for Ti-fumaric acid hybrid films deposited at different temperatures from 180 to 350 °C; (b) Thickness of hybrid films versus number of ALD/MLD cycles at 200 °C.

The film thickness of Ti–fumaric acid versus the deposition cycles was also examined at a fixed deposition temperature of 200 °C, as seen in Figure 3(b). The film thickness is linearly dependent on the number of cycles, which is one of typical features of ALD mechanism.

The topology and surface roughness of Ti-fumaric acid hybrid thin films deposited at various temperatures for 200 cycles have been examined, as recorded in Figure 4. The hybrid films in the range of thickness from 9.8 to 21.9 nm show very smooth surfaces with small RMS values of ~0.59-0.76 nm at 300 °C and below. The 3×3 μm^2 images were

Dalton Transactions Accepted Manuscript

used for acquiring the RMS values to obtain good statistics. A slow increment in roughness can be observed under 300 °C, however, the film roughness increases quickly to 1.42 nm at 350 °C, suggesting the plausible significant change of hybrid structure.

XRD scans of Ti-fumaric acid hybrid thin films deposited at 180-350 °C show no diffraction peaks. It is consistent with amorphous titanicone, alucone and zincone films from literature reports.[6-7,10,19]

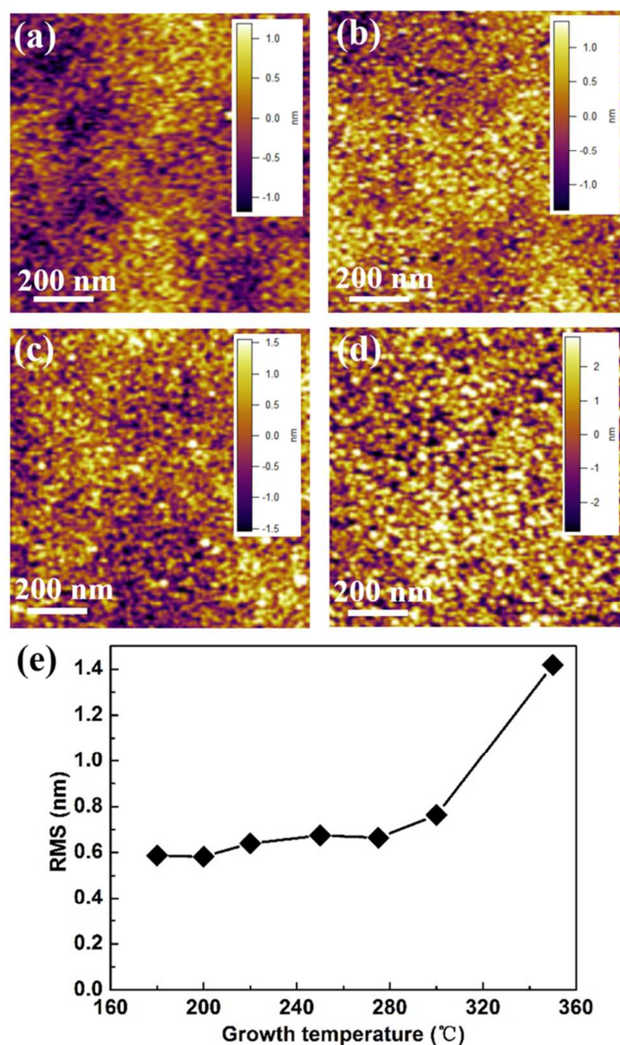

Figure 4. AFM images (1 μm×1 μm) for Ti–fumaric acid hybrid films deposited at (a) 200 °C, (b) 250 °C, (c) 300 °C and (d) 350 °C. (e) RMS values at different temperatures from 180 to 350 °C, which were obtained from 3 μm×3 μm AFM images.

Dalton Transactions Accepted Manuscript

In addition, the refractive index of 200 cycles hybrid films grown at 200 °C was also evaluated, as seen in Figure 5. The titanicones films exhibit the refractive index of 1.8 at 590 nm, which is nearly the same as this value of Ti hybrid films deposited using $TiCl_4$ and EG.[19] The refractive index of titanicone films is much lower than that of 2.4 at 590 nm of the ALD-derived TiO_2 films.[19] Compared with the parent metal oxides, a lowering of the refractive index for the metalcones has also been observed in other metalcones.[7,19] It can be ascribed to the fact that the density of the hybrid films is smaller than the parent metal oxides because of the organic species.

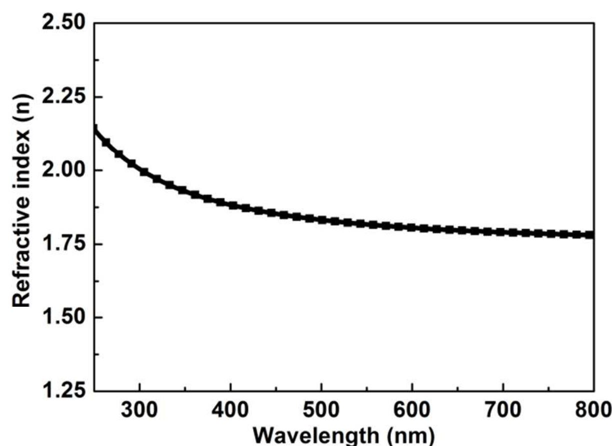

Figure 5. Refractive index (n) versus wavelength for the 200 cycles hybrid film grown at 200 °C.

3.2. Composition and Growth Mechanism of Ti-fumaric Acid Hybrid Films.

In order to characterize the chemical state and composition of the hybrid films deposited at various temperatures, the narrow-scan XPS analyses were performed. Figure 6 shows the XPS spectra of C 1*s*, O 1*s*, Ti 2*p* and Cl 2*p* of the hybrid films at different deposition temperatures. In Figure 6(a), except the sample deposited at 350 °C, all the samples display the significant two peaks centered at about 284.6 and 288.5 eV, corresponding to the C-C (backbone chain carbon) and O-C=O (carboxyl) bonds from C

Dalton Transactions Accepted Manuscript

1*s*, respectively.[48] And the O-C=O bond intensity shows the tendency of slow decrease with increasing the deposition temperature to 300 °C. However when deposition temperature reaches 350 °C, the O-C=O bond intensity dramatically becomes very weak.

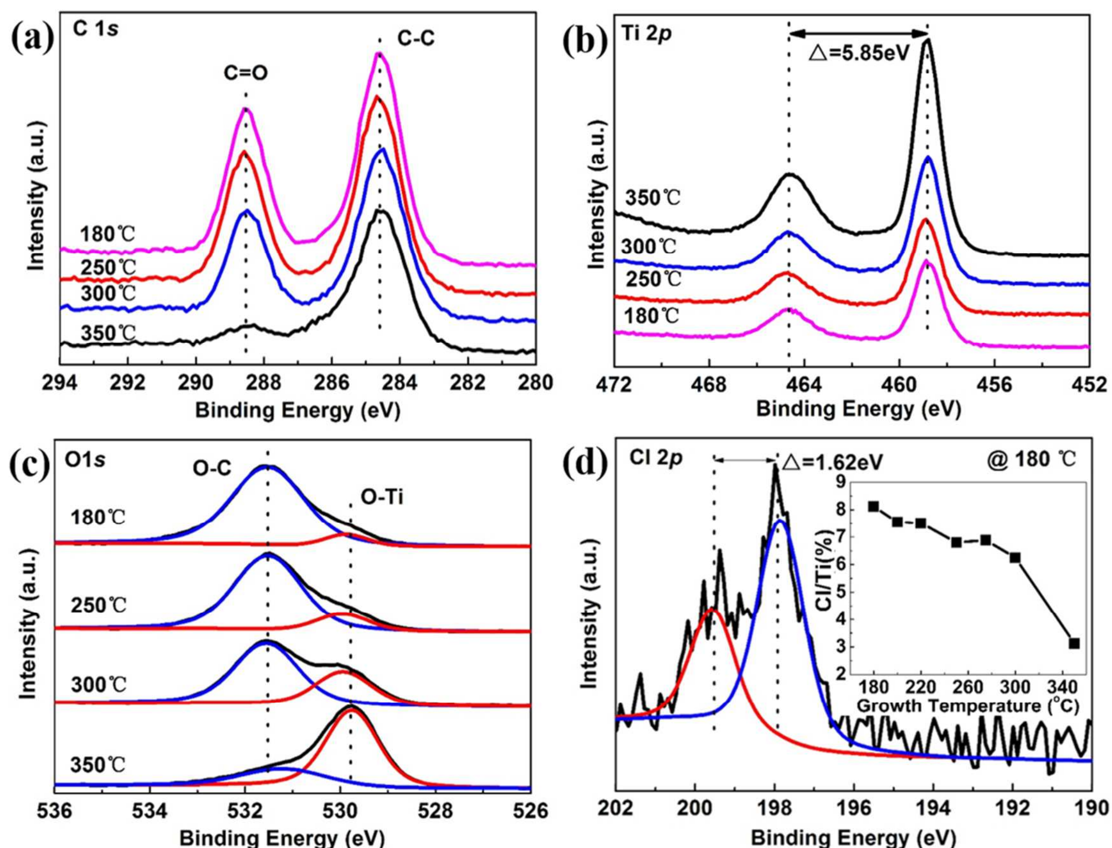

Figure 6. XPS spectra of (a) C 1*s*, (b) Ti 2*p*, (c) O 1*s* and (d) Cl 2*p* of hybrid films deposited at various temperatures. The inset of (d) is the Cl/Ti atomic ratio percentage versus deposition temperature.

In Figure 6(b), the doublet at 464.7 and 458.8 eV can be assigned to Ti $2p_{1/2}$ and Ti $2p_{3/2}$ peaks of Ti-O bonds with the spin orbit splitting energy of 5.85 eV, in consistent with literature value of TiO_2.[49] When raising the deposition temperature, the Ti 2*p* peak position keeps constant, however, the peak intensity is enhanced, especially for 350 °C

Dalton Transactions Accepted Manuscript

sample with a sudden increase. There are two peaks located at 529.8 and 531.5 eV in Figure 6(c), representing the O-Ti and O-C bonds from O 1*s*, respectively.[50] It is found that the O-Ti intensity increases and correspondingly the O-C intensity decreases with increasing the deposition temperature. The O-C intensity is much greater than the O-Ti one at 180 ^{o}C whereas the O-Ti intensity is much higher than the O-C one at 350 ^{o}C.

Figure 6(d) shows the Cl 2*p* XPS spectrum of the hybrid film deposited at 180 °C. The doublet at 197.9 and 199.5 eV with stronger background noise can be ascribed to Cl $2p_{1/2}$ and Cl $2p_{3/2}$ peaks with the spin orbit splitting energy of 1.6 eV, revealing that there is some residual Cl embedded in the hybrid films. The Cl content (atomic ratio of Cl/Ti) shows slow decline from 8% to 6% with increasing the deposition temperature from 180 °C to 300 °C and a sudden drop to 3% at 350 °C, as seen in the inset of Figure 6(d). Compared to the literature value (Cl/Ti ratio) of 36-44% in Ti-EG hybrid films and 15-35% in Ti- 4,4_-oxydianiline (Ti-ODA) hybrid films,[17,19] the Cl impurity of 3-8% is much lower in Ti–fumaric acid hybrid films. It is ascribed to the effect of various functional groups in organic precursors. The higher Cl presence in Ti-EG films comes from the probability of "double reactions" between $TiCl_4$ and EG.[19] The Cl impurity in Ti-ODA may be related to some amounts of Cl from $TiCl_4$ that has not reacted with ODA or from residual HCl that has absorbed into the film.[17] Here, the slight Cl residue in Ti–fumaric acid films can be attributed to tiny unreacted Ti-Cl species with fumaric acid or absorbed HCl.

The dependence of atomic ratio of $O_{Ti\text{-}O}/O_{C\text{-}O}$ and $O_{Ti\text{-}O}/Ti$ of Ti–fumaric acid films on deposition temperature, calculated from the O 1*s* and Ti 2*p* XPS spectra, is shown in Figure 7(a) and (b), respectively. The atomic ratio of $O_{Ti\text{-}O}/O_{C\text{-}O}$ is only 0.09-0.13 at

Dalton Transactions Accepted Manuscript

deposition temperature of 180-220 ^{o}C and 0.19-0.49 at 250-300 ^{o}C, indicating that only slight O atoms in the films are bonded to Ti atoms at lower growth temperature. When deposition temperature reaches 350 ^{o}C, the ratio of $O_{Ti\text{-}O}/O_{C\text{-}O}$ dramatically increases to 2.83, suggesting that there are lots of O atoms bonded to Ti atoms instead of C atoms. The ratio of $O_{Ti\text{-}O}$/Ti increases from 0.6 to 1.5 with deposition temperature from 180 ^{o}C to 300 ^{o}C. Especially, the hybrid film deposited at 350 ^{o}C shows the ratio of $O_{Ti\text{-}O}$/Ti of 2.04, which almost equals to the theoretical value in TiO_2 films.

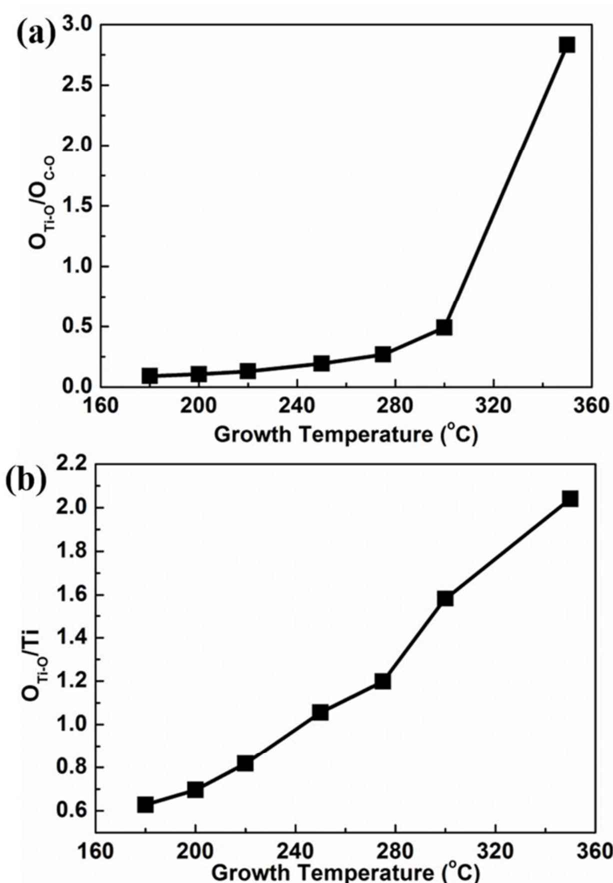

Figure 7. The atomic ratio of (a) $O_{Ti\text{-}O}/O_{C\text{-}O}$ and (b) $O_{Ti\text{-}O}$/Ti determined by XPS spectra for Ti–fumaric acid films deposited at various temperatures. $O_{Ti\text{-}O}$ and $O_{C\text{-}O}$ refer to O atoms bonded to Ti and C, respectively.

The effect of the deposition temperature on the hybrid film composition of C: O: Ti: Cl

Dalton Transactions Accepted Manuscript

has been summarized in Table 1 with the normalized Ti composition setting to 1.00. It is clearly seen that with raising the reaction temperature from 180 °C to 350 °C, all the C, O and Cl contents show declining tendency. For 180, 200 and 220 °C samples, the relative composition ratio is almost close with smaller deviation of C: O: Ti=8.10:7.25:1.00 at 200 °C. When further enhancing deposition temperature to 250, 275 and 300 °C, the C and O components decrease steadily. For 350 °C sample, a remarkable composition change in C: O: Ti=1.97:2.76:1.00 is confirmed.

Table 1 XPS compositional ratio of hybrid films deposited at various temperatures

Deposition T (^{o}C)	Atomic ratio			
	C	O	Ti	Cl
180	8.35	7.49	1.00	0.08
200	8.10	7.25	1.00	0.08
220	7.80	7.10	1.00	0.08
250	7.06	6.50	1.00	0.07
275	6.06	5.66	1.00	0.07
300	4.66	4.80	1.00	0.06
350	1.97	2.76	1.00	0.03

The proposed two-step half-reactions between $TiCl_4$ and fumaric acid can be written as follows:

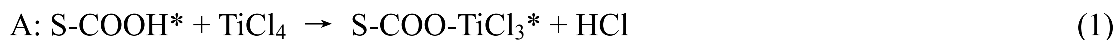

A: $\text{S-COOH}^* + \text{TiCl}_4 \rightarrow \text{S-COO-TiCl}_3^* + \text{HCl}$ (1)

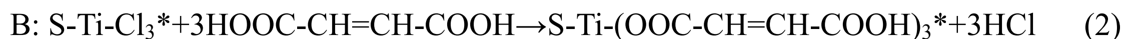

B: $\text{S-Ti-Cl}_3^*\text{+3HOOC-CH=CH-COOH} \rightarrow \text{S-Ti-(OOC-CH=CH-COOH)}_3^*\text{+3HCl}$ (2)

The S refers to the substrate with the reaction products from the previous reactions and the asterisk denotes the surface species. As known, there exist 3 kinds of possible bonding situations of bidentate, unidentate, and bridging complexes between metal ions and carboxyl group,[51, 52] as illustrated in Fig. 8.

Dalton Transactions Accepted Manuscript

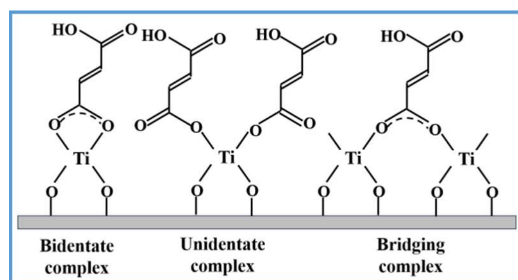

Figure 8. The possible bonding situations of bidentate, unidentate, and bridging complexes between Ti^{4+} and fumaric acid group.

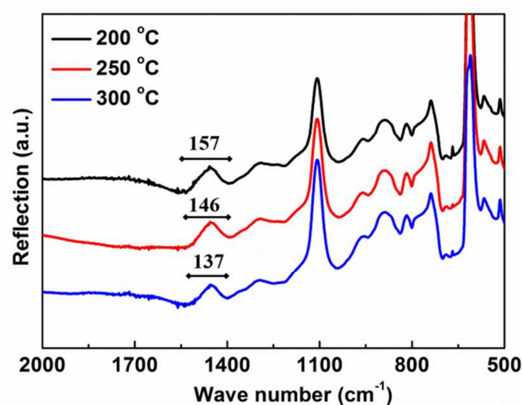

Figure 9. FTIR spectra of Ti-fumaric acid films deposited on Si at 200, 250 and 300 °C. The wave number splitting (cm^{-1}) between the asymmetric and symmetric carboxylate bands (Δ) are denoted.

In order to characterize the actual bonding mode in the hybrid films, the FTIR spectra of hybrid films deposited at various temperatures were measured and shown in Figure 9. Absorption bands related to carboxylate groups, such as the asymmetric stretch around 1600 cm^{-1} and symmetric stretch just below 1500 cm^{-1}, are visible in all spectra. The widths of the frequency splitting between these two bands are indicated in Figure 9. A splitting between the asymmetric and symmetric carboxylate stretching bands (Δ) in the range 50-150 cm^{-1} is typical for bidentate complexes, bridging complexes have Δ in the range 130-200 cm^{-1}, and unidentate complexes have $\Delta > 200$ cm^{-1}.[53]

The hybrid film obtained at 200 °C shows Δ of ~157 cm^{-1}, indicating the bridging bonding mode. When further increasing the deposition temperature to 250 °C and 300 °C,

Dalton Transactions Accepted Manuscript

the Δ decreases to 146 cm^{-1} and 137 cm^{-1}, suggesting a mixture of bidentate and bridging bonding mode in the hybrid films. When the interaction of $TiCl_4$ and fumaric acid is bridging complex or bidentate/bridging mixture, the corresponding repeating unit should be $(\text{-Ti-O-CO-CH=CH-CO-O})_n$ with the nominal composition ratio of C: O: Ti=4:4:1. However there is a higher concentration of C and O in our hybrid films, especially at the lower deposition temperature. It may be ascribed to the incorporation of some organic molecules in the hybrid films caused by physisorption at lower deposition temperature. Similar phenomenon has been observed in trimethyl aluminum (TMA)-glycidol system with an evidently increased organic fraction at reduced temperature.[15] In addition, the temperature-dependent composition may be related to the temperature-dependent density of reactive sites (-OH) . At low temperature, the fumaric acid molecules adsorbed on the surface might form some hydrogen bond between the carboxyl groups (–COOH), leading to the reduction of active sites of hydroxyl group (-OH) after fumaric acid dosing. As a result, less $TiCl_4$ are adsorbed on the growth surface to form Ti-O bond during the subsequent $TiCl_4$ pulse.

At 350 °C, a dramatic decrease in C and O elements with C: O: Ti ratio of 1.97:2.76:1.00 shows the hybrid structure has been degraded substantially, implying the thermal decomposition of fumaric acid precursor, in consistent with as-mentioned increased growth rate and surface roughness of hybrid films. The fumaric acid decomposes at high temperature, which produces the byproduct of H_2O. H_2O could react with Ti-Cl, resulting in the formation of more Ti-O bonds.

In order to characterize the thermal stability of fumaric acid, we have performed gas chromatography-mass spectrometry (GC-MS) measurement of fumaric acid dissolved in

Dalton Transactions Accepted Manuscript

ethanol at 200 and 300 ^{o}C, respectively. The GC-MS results show that there exists only fumaric acid molecule at 200 ^{o}C however some maleic anhydride (cis-butenedioic anhydride) is detected besides fumaric acid at 300 ^{o}C. It indicates that some fumaric acid molecules (~10%) form maleic anhydride by splitting off H_2O at 300 ^{o}C, as seen in Eq. 3.

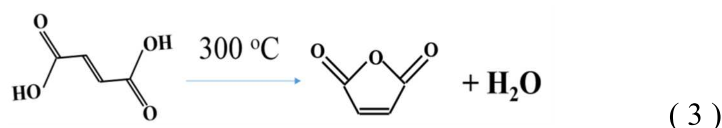

(3)

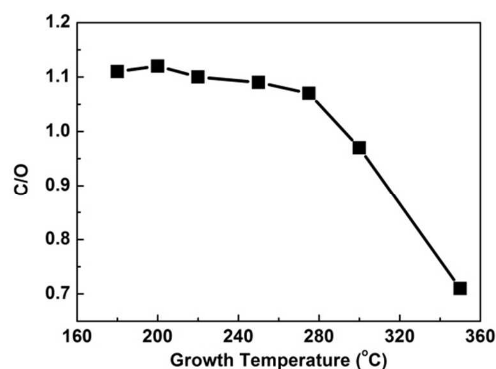

Figure 10. The atomic ratio of C/O determined by XPS spectra for Ti-fumaric acid films deposited at various temperatures.

Figure 10 shows the atomic ratio of C/O for Ti-fumaric acid films deposited at various temperatures. It is found that the atomic ratio of C/O basically keeps constant at ~1.1 ranging from 180 ^{o}C to 270 ^{o}C. Because both C and O elements in hybrid films come from the organic precursor of fumaric acid, this also confirms the thermal stability of fumaric acid below 300 ^{o}C, in consistent with TG-DSC result in Fig.1. However, when the deposition temperature is raised to 300 ^{o}C and 350 ^{o}C, the C/O ratio decreases to 0.97 and 0.71, respectively. It indicates that the fumaric acid begins to show a tendency of thermal decomposition at 300 ^{o}C and the significant thermal decomposition appears at 350 ^{o}C. The yielded by-product H_2O changes the reaction mechanism for $TiCl_4$-fumaric acid system at high temperature, resulting in the formation of more Ti-O bonds.

Dalton Transactions Accepted Manuscript

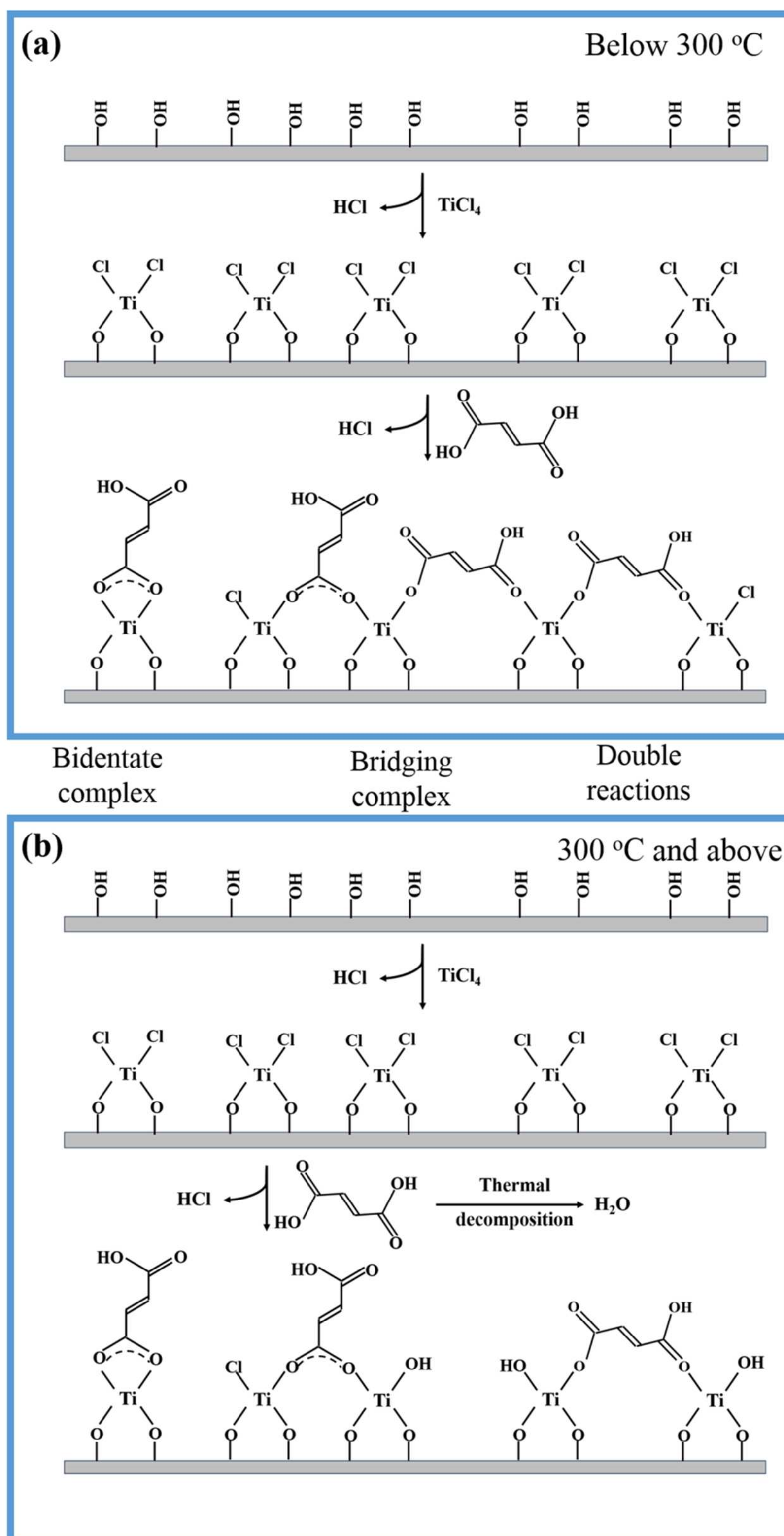

Figure 11. Illustration of possible reaction mechanism for $TiCl_4$-fumaric acid system (a) below 300 °C, (b) 300 °C and above.

Dalton Transactions Accepted Manuscript

Therefore the $TiCl_4$/fumaric acid process exhibits the temperature-dependant composition behavior, which can be attributed to the more organic incorporation into the hybrid films at lower deposition and temperature-dependant density of reactive sites (-OH) below 300 ^{o}C. However, at 300 ^{o}C and above, the influence of thermal decomposition of fumaric acid on composition and hybrid structure has to be considered. Besides, considering the double reactions,[19] the schematic of possible reaction mechanism for $TiCl_4$-fumaric acid system is proposed, as shown in Figure 11.

3.3. Stability of Ti-fumaric Acid Hybrid Films and Thermal-induced TiO_2 Nanoparticles.

The stability of the hybrid films were firstly explored by chemical treatment. The hybrid films deposited at 200 ^{o}C were immerged in ethanol, isopropanol, acetone and deionized water for 1 h, respectively. All the samples show two main peaks centered at 529.8 and 531.5 eV, corresponding to the O-Ti and O-C bond, respectively, as shown in Figure S2. The table II illustrates the O-C/O-Ti atom percentage and the atom ration of O-Ti to O-C for the hybrid films with different treatments. The atom percentage of the O-C and O-Ti keeps unchanged basically after organic solvent dipping treatment, indicating good stability of the hybrid films in these organic solvents. However, the hybrid film shows poor stability in deionized water. The O-C percentage decreases sharply and the O-Ti percentage increases obviously after 1h water dipping treatment. In order to investigate the storage stability of Ti-fumaric acid films, we placed as-deposited sample by vacuum-packing. After sealed-storage for 20 months, the XPS analyses of the hybrid films were performed. The atom percentage exhibits similar tendency with the sample immersed in water in relatively mild mode. It can be ascribed to the fact that

Dalton Transactions Accepted Manuscript

hybrid films reacted with the water from air leakage. Another change is the declining chlorine content from the Cl/Ti ratio of 8% to 3% due to the reaction with water[24] or the HCl evaporation.

Table 2 The O-C, O-Ti percentage and the ratio of O-Ti to O-C for the hybrid films with different treatments

Treatments	O-C (%)	O-Ti (%)	Ratio of O-Ti/O-C
As deposited	77.80	22.20	0.28
Ethanol	79.03	20.97	0.26
Isopropanol	77.86	22.14	0.28
Acetone	80.98	19.02	0.23
DI water	32.17	67.83	2.11
Stored for 20 months by vacuum-package	63.93	36.07	0.56

It can be found that most O atoms bonded to C transform into O atoms bonded to Ti atoms after water dipping treatment. It can be ascribed the fact that hybrid films could react with the H_2O, resulting in the O-Ti bonds formation, as shown in Eq.4. Similar phenomena have been observed in quite a few organic-inorganic hybrid thin films.[54,55]

$$\text{-Ti-O-CO-} + H_2O \rightarrow \text{-Ti-OH} + \text{-CO-OH} \quad (4)$$

According to this reaction, the hybrid films can finally be transformed into porous metal oxides, which has been verified in Al-based hybrid films.[54,55]

The thermal stability of the hybrid films were also examined by post-deposition annealing. The hybrid films were annealed at 400, 600 and 850 °C for 10 s in air by RTA with the heating rate of 50 °C/s. Figure 12 shows the C 1s spectra of the as-deposited

Dalton Transactions Accepted Manuscript

sample and the ones annealed at 400, 600 and 850 °C. It can be found that the peak intensity from both C-C bonds and O-C=O bonds decrease after 400 °C thermal treatment, indicating the poor thermal stability of the hybrid films. It is easily understood due to the thermal decomposition of organic species in hybrid films. When the annealing temperature is 600 °C and above, there is no O-C=O bonds peak in hybrid films. XPS measurements were also carried out for the 600 °C annealed sample after Ar-ion sputtering so as to avoid the effect of sample surface contamination. After etching, there is no peak from C 1s, implying that RTA at 600 °C can remove the organic parts in the hybrid films effectively to obtain inorganic TiO_2.

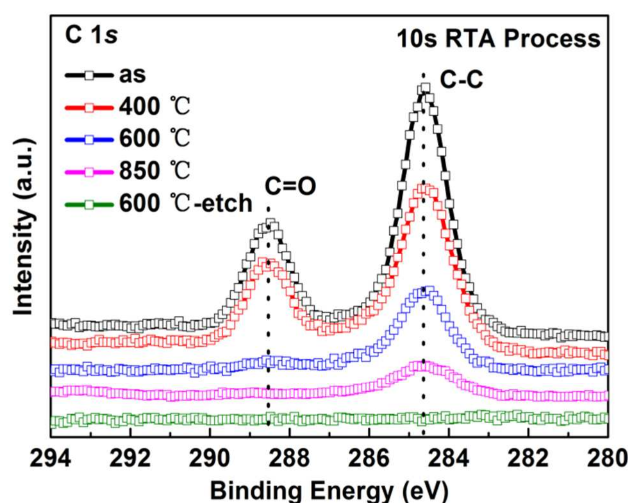

Figure 12. C 1s spectra of the as-deposited sample and the ones annealed at 400, 600 and 850 °C for 10 s by RTA.

In order to further characterize the effect of various thermal treatments and the film thickness on the topography of TiO_2 derived from hybrid films, the Ti-based hybrid films were annealed at 850 °C in air for 10 s by RTA with a ramp rate of 50 °C/s and for 30 min by CFA with a ramp rate of 30 °C/min, respectively. Figure 13 shows the AFM images of hybrid films with various cycles of 50, 100, and 200 cycles annealed at 850 °C by 10s

Dalton Transactions Accepted Manuscript

RTA and 30 min CFA. Moreover, RTA and CFA result in TiO_2 nanoparticles with different topographic features. Compared with CFA, RTA yields smaller TiO_2 nanoparticles (~15 nm in diameter) with uniform size distribution and higher nanocrystal area density. The TEM image of the RTA treated sample also confirms the formation of TiO_2 nanoparticles with rutile phase, as shown in Figure S4. Meanwhile, the thickness of original hybrid films has no effect on the RTA-derived nanoparticle size. It is attributed to the fact that 10 s RTA with higher heating rate of 50 ^oC/s leads to rapid nucleation and leaves no time for TiO_2 particles to grow larger. Conventional tube furnace annealing with a slow heating rate of 30 ^oC/min and a longer duration time of 30 min produces large TiO_2 particles on Si substrates. For the hybrid films with 50, 100 and 200 cycles, the average diameter of the CFA-derived TiO_2 nanoparticles is ~20, 25 and 33 nm, respectively. The thicker the original hybrid films are, the larger the formed TiO_2 nanoparticles are. Above all, we can tune the size and density of TiO_2 particles on substrates by choosing proper thermal treatment process and hybrid film thickness.

Dalton Transactions Accepted Manuscript

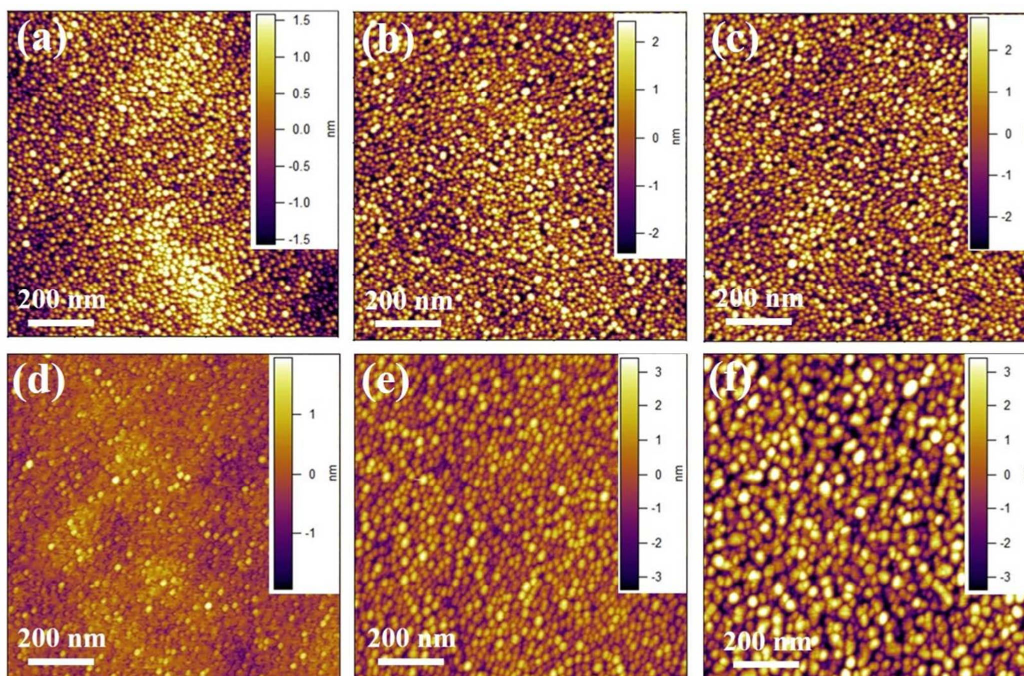

Figure 13. AFM images of hybrid films with (a)/(d) 50 cycles, (b)/(e) 100 cycles and (c)/(f) 200 cycles annealed at 850 ^{o}C by (a)/(b)/(c) 10 s RTA and (d)/(e)/(f) 30 min CFA.

3.4. Charge Trapping Ability of Ti-fumaric Acid Hybrid Films.

In order to detect the charge trapping ability of the hybrid films, we fabricated a flash memory capacitor structure comprised of a top electrode, blocking oxide, charge trapping layer (CTL), tunnel oxide and p-Si substrate.[56] Here we used the Ti-based hybrid films as a CTL. In our memory capacitor, except for the Pt top electrode, all layers of blocking oxide (15 nm-thick Al_2O_3), CTL (Ti-based hybrid film at 200 ^{o}C with various thicknesses from 1 nm to 10 nm), and tunnel oxide (6 nm-thick Al_2O_3) were continuously grown on *p*-Si without breaking vacuum of the ALD reactor, which is an important advantage of our memory structure in terms of fabrication. Figure 14 shows the high frequency C-V curves of the samples with (a) 1 nm, (b) 4 nm, (c) 7 nm and (d) 10 nm CTL with different sweeping voltages. The memory windows enlarge with the increase of the sweeping

Dalton Transactions Accepted Manuscript

voltage. 10 nm sample shows a largest memory window of 5.85 V when the sweeping gate voltage is ±12 V. As the sweeping voltage increases to ±14 V, the memory window of 10 nm sample reaches a larger value of 8.01 V, indicating a good charge-storage capability. The CTL thickness of Ti-based hybrid films plays a key role in the charge-storage capability. The thicker the Ti-based hybrid film is, the better charge-storage capability the sample shows.

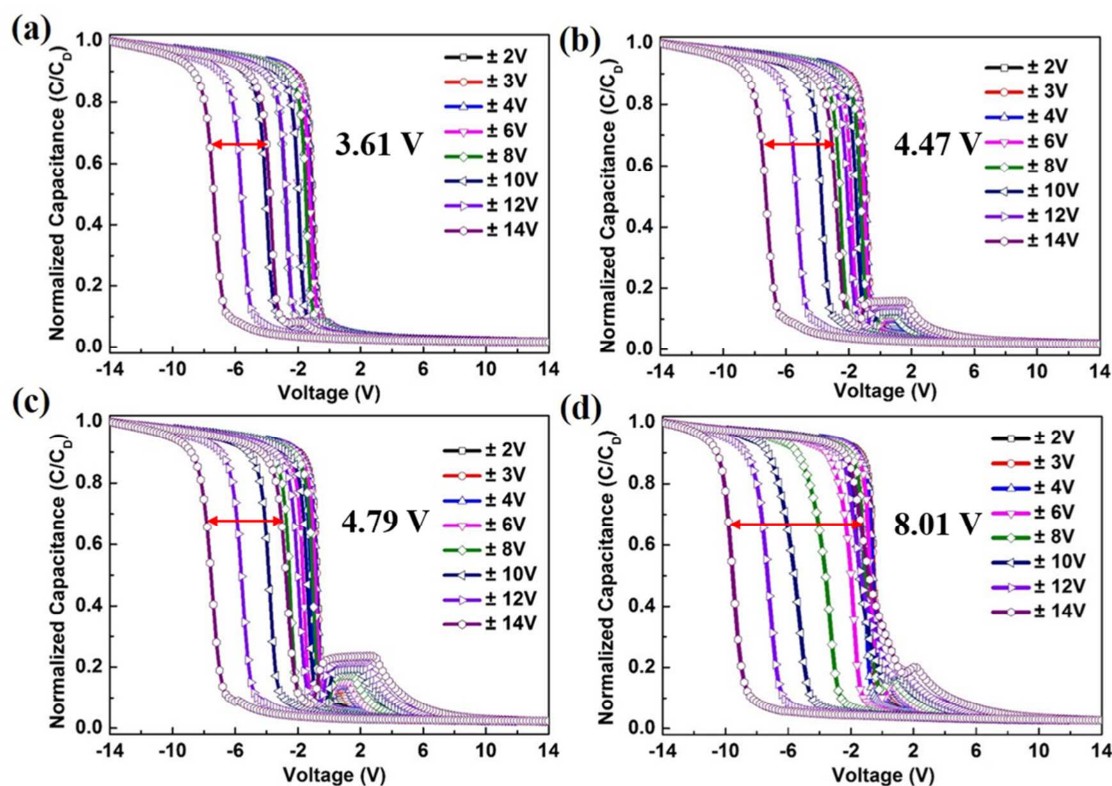

Figure 14. High frequency C-V curves of the samples with (a) 1 nm, (b) 4 nm, (c) 7 nm and (d) 10 nm CTL with different sweeping voltages.

4. CONCLUSION

Ti-fumaric acid hybrid thin films were successfully grown using $TiCl_4$ and fumaric acid precursors by MLD. The impact of deposition temperatures on the growth rate, morphology, and composition of hybrid films has been characterized systematically. The

Dalton Transactions Accepted Manuscript

MLD process of the hybrid films shows self-limiting surface reaction with a reasonable growth rate of ~0.93 Å per cycle and very smooth surface of ~0.58 nm RMS values at 200 ^{o}C. A temperature-dependent film growth behavior has been observed in hybrid films. The growth rate reduces from 1.10 to 0.49 Å/cycle and the film composition of C:O:Ti ratio varies from 8.35:7.49:1.00 to 4.66:4.80:1.00, when increasing deposition temperature from 180 ^{o}C to 300 ^{o}C. FTIR spectra indicates the hybrid film shows bridging bonding mode at low deposition temperature of 200 °C and bridging/bidentate mixture bonding mode at elevated deposition temperature of 250 and 300 °C. The higher C and O amount deviated from ideal composition may be ascribed to the more organic incorporation in to the hybrid film and temperature-dependant density of reactive sites (-OH) below 300 ^{o}C. The composition of hybrid films grown at 350 °C show a dramatic decrease in C and O elements (C: O: Ti=1.97:2.76:1.00) due to the thermal decomposition of fumaric acid precursor. The produced by-product H_2O changes the structure of hybrid films, resulting in the formation of more Ti-O bonds at high temperature. The stability of hybrid films against chemical and thermal treatment, and long-time storage by vacuum-packing was also explored carefully. The hybrid films shows good stability in some organic solvent, however, they suffer from poor stability in H_2O or after sealed-storage for 20 month due to the reaction with H_2O, resulting in the O-Ti bonds formation. The hybrid film can be transformed into TiO_2 nanoparticles via various post deposition annealing with different grain size and density. Moreover, the charge trapping ability of the hybrid film is verified by a charge trapping memory capacitor in which the hybrid film was inserted as a charge trapping layer. The thicker the charge trapping layer of Ti-based hybrid films is, the better charge-storage capability the

Dalton Transactions Accepted Manuscript

sample shows.

ACKNOWLEDGMENTS

This project is supported by the Natural Science Foundation of China (51202107), a grant from the State Key Program for Basic Research of China (2015CB921203 and 2011CB922104). Ai-Dong Li also thanks the support of Priority Academic Program Development in the Jiangsu Province and the Doctoral Fund of Ministry of Education of China (20120091110049). We also thank the support of Colleges and Universities in Jiangsu Province plans to graduate research and innovation (CXZZ13_0049).

Dalton Transactions Accepted Manuscript

REFERENCES

1 A. M. Shevjakov, G. N. Kuznetsova and V. B. Aleskovskii, in *Chemistry of High-Temperature Materials,* Proceedings of the Second USSR Conference on High-Temperature Chemistry of Oxides, Leningrad, USSR, 26-29 November 1965 (Nauka, Leningrad, USSR, 1967), pp. 149-155, in Russian.

2 T. Suntola and J. Antson, *US. Patent,* 1977, 4,058,430.

3 R. L. Puurunen, *J. Appl. Phys.,* 2005, **97,** 121301.

4 S. M. George, *Chem. Rev.,* 2010, **110,** 111-131.

5 O. Nilsen and H. Fjellvåg, 2006, *WO*2006071126.

6 O. Nilsen, K. B. Klepper, H. Ø. Nielsen and H. Fjellvåg, *ECS Trans.*, 2008, **16**, 3-14.

7 A. A. Dameron, D. Seghete, B. B. Burton, S. D. Davidson, A. S. Cavanagh, J. A. Bertrand and S. M. George, *Chem. Mater.*, 2008, **20**, 3315-3326.

8 X. Liang, D. M. King, P. Li, S. M. George and A. W. Weimer, *AIChE J.*, 2009, **55**, 1030-1039.

9 Q. Peng, B. Gong, R. M. VanGundy and G. N. Parsons, *Chem. Mater.*, 2009, **21**, 820-830.

10 B. Yoon, J. L. O'Patchen, D. Seghete, A. S. Cavanagh and S. M. George, *Chem. Vapor Depos.*, 2009, **15**, 112-121.

11 B. Yoon, D. Seghete, A. S. Cavanagh and S. M. George, *Chem. Mater.*, 2009, **21**, 5365-5374.

12 S. M. George, B. Yoon and A. A. Dameron, *Acc. Chem. Res.*, 2009, **42**, 498-508.

13 K. B. Klepper, O. Nilsen and H. Fjellvag, *Dalton Trans.*, 2010, **39**, 11628–11635.

Dalton Transactions Accepted Manuscript

14 K. B. Klepper, O. Nilsen, P.-A. Hansen and H. Fjellvag, *Dalton Trans.*, 2011, **40**, 4636-4646.

15 K. B. Klepper, O. Nilsen, T. Levy and H. Fjellvag, *Eur. J. Inorg. Chem.*, 2011, **34**, 5305-5312.

16 S. M. George, B. H. Lee, B. Yoon, A. I. Abdulagatov and R. A. Hall, *J. Nanosci. Nanotechnol.*, 2011, **11**, 7948-7955.

17 A. Sood, P. Sundberg, J. Malm and M. Karppinen, *Appl. Surf. Sci.*, 2011, **257**, 6435-6439.

18 B. Gong, Q. Peng and G. N. Parsons, *J. Phys. Chem. B*, 2011, **115**, 5930-5938.

19 A. I. Abdulagatov, R. A. Hall, J. L. Sutherland, B. H. Lee, A. S. Cavanagh and S. M. George, *Chem. Mater.*, 2012, **24**, 2854-2863.

20 S. Ishchuk, D. H. Taffa, O. Hazut, N. Kaynan and R. Yerushalmi, *ACS Nano*, 2012, **6**, 7263-7269.

21 A. Sood, P. Sundberg and M. Karppinen, *Dalton Trans.*, 2013, **42**, 3869-3875.

22 L. D. Salmi, M. J. Heikkilä, E. Puukilainen, T. Sajavaara, D. Grosso and M. Ritala, *Microporous Mesoporous Mater.*, 2013, **182**, 147-154

23 K. B. Klepper, O. Nilsen, S. Francis and H. Fjellvag, *Dalton Trans.*, 2014, **43**, 3492-3500.

24 P. Sunberg and M. Karppinen, *Eur. J. Inorg. Chem.*, 2014, **6**, 968-974.

25 B. H. Lee, V. R. Anderson and S. M. George, *ECS Trans.,* 2011, **41**, 131-138.

26 D. B. Mitzi, *Chem. Mater.,* 2001, **13,** 3283-3298.

27 C. Y. Kao, B. Li, Y. Lu, J. W. Yoo and A. J. Epstein, *J. Mater. Chem. A,* 2014, **2,**

Dalton Transactions Accepted Manuscript

6171-6176.

28 A. Bétard and R. A. Fischer, *Chem. Rev.*, 2012, **112**, 1055-1083.

29 D. Bersani, P. P. Lottici, M. Casalboni, A. Bétard, R. A. Fischer and P. Prosposito, *Mater. Lett.*, 2001, **51**, 208-212.

30 Y. H. Li, H. J. Zhang, S. B. Wang, Q. G. Meng, H. R. Li and X. H. Chuai, *Thin Solid Films*, 2001, **385**, 205-208.

31 Z. Y. Cheng, H. F. Wang, Z. W. Quan, C. K. Lin, J. Lin and Y. C. Han, *J. Cryst. Growth*, 2005, **285**, 352-357.

32 K. H. Haas, S. Amberg-Schwab, K. Rose and G. Schottner, *Surf. Coat. Technol.*, 1999, **111**, 72-79.

33 Z. L. Xiao, H. Z. Chen, M. M. Shi, G. Wu, R. J. Zhou, Z. S. Yang, M. Wang and B.-Z. Tang, *Mater. Sci. Eng., B*, 2005, **117**, 313-316.

34 C. R. Kagan, D. B. Mitzi and C. D. Dimitrakopoulos, *Science*, 1999, **286**, 945-947.

35 C. C. Chang and W. C. Chen, *Chem. Mater.*, 2002, **14**, 4242-4248.

36 A. Kobayashi, H. Naito, Y. Matsuura, K. Matsukawa, S. Nihonyanagi and Y. Kanemitsu, *J. Non-Cryst. Solids*, 2002, **299–302**, 1052-1056.

37 E. J. Nassar, R. R. Gonçalves, M. Ferrari, Y. Messaddeq and S. J. L. Ribeiro, *J. Alloys Compd.*, 2002, **344**, 221-225.

38 B. Darracq, F. Chaput, K. Lahlil, J.-P. Boilot, Y. Levy, V. Alain, L. Ventelon and M. Blanchard-Desce, *Opt. Mater.*, 1998, **9**, 265-270.

39 M. Minelli, M. G. De Angelis, F. Doghieri, M. Marini, M. Toselli and F. Pilati, *Eur. Polym. J.*, 2008, **44**, 2581-2588.

Dalton Transactions Accepted Manuscript

40 B. H. Lee, K. H. Lee, S. Im and M. M. Sung, *J. Nanosci. Nanotechnol.*, 2009, **9**, 6962-6967.

41 K. Chondroudis and D. B. Mitzi, *Chem. Mater.*, 1999, **11**, 3028-3030.

42 D. B. Mitzi, C. D. Dimitrakopoulos and L. L. Kosbar, *Chem. Mater.*, 2001, **13**, 3728-3740.

43 M. Era, S. Morimoto, T. Tsutsui and S. Saito, *Appl. Phys. Lett.*, 1994, **65**, 676-678.

44 G. L. Graff, R. E. Williford and P. E. Burrows, *J. Appl. Phys.,* 2004, **96,** 1840-1849.

45 A. L. Linsebigler, G. Q. Lu and J. T. Yates, *Chem. Rev.,* 1995, **95,** 735-758.

46 U. Bach, D. Lupo, P. Comte, J. E. Moser, F. Weissortel, J. Salbeck, H. Spreitzer and M. Gratzel, *Nature,* 1998, **395,**, 583-585.

47 P. Sundberg and M. Karppinen, *Beilstein J. Nanotechnol.,* 2014, **5,** 1104-1136.

48 D. Briggs and G. Beamson, *Anal. Chem.,* 1992, **64,** 1729-1736.

49 P. R. Moses, L. M. Wier, J. C. Lennox, H. O. Finklea, F. R. Lenhard and R. W. Murray, *Anal. Chem.,* 1978, **50,** 576-585.

50 L. J. Gerenser, *J. Vac. Sci. Technol. A,* 1990, **8,** 3682-3691.

51 H. Hu, J. Saniger, J. Garcia-Alejandre and V. M. Castano, *Mater. Lett.,* 1991, **12,** 281-285.

52 W. Wang, J. W. Zhang, H. Z. Huang, Z. S. Wu and Z. J. Zhang, *Appl. Surf. Sci.,* 2007, **253**, 5393-5399.

53 F. Verpoort, T. Haemers, P. Roose and J. P. Maes, *Appl. Spectrosc.,* 1999, **53,** 1528-1534.

54 X. H. Liang, M. Yu, J. Li, Y. B. Jiang and A. W. Weimer, *Chem. Commun.,* 2009, **46,** 7140-7142.

Dalton Transactions Accepted Manuscript

55 X. H. Liang, B. W. Evanko, A. Izar, D. M. King, Y. B. Jiang and A. W. Weimer, *Micropor. Mesopor. Mat.,* 2013, **168,** 178-182.

56 P. C. Y. Chen, *IEEE Trans. Electron Devices,* 1977, **ED-24,** 584-586.

Dalton Transactions Accepted Manuscript